LETTERS
https://doi.org/10.1038/s41587-020-0470-y

nature biotechnology

Check for updates

Combinatorial single-cell CRISPR screens by direct guide RNA capture and targeted sequencing

Joseph M. Replogle[1,2,3,4,5], Thomas M. Norman[3,4,5,10], Albert Xu[1,3,4,5], Jeffrey A. Hussmann[3,4,5,6], Jin Chen[3,4,5], J. Zachery Cogan[3,4,5], Elliott J. Meer[7], Jessica M. Terry[7], Daniel P. Riordan[7], Niranjan Srinivas[7], Ian T. Fiddes[7], Joseph G. Arthur[7], Luigi J. Alvarado[7], Katherine A. Pfeiffer[7], Tarjei S. Mikkelsen[7], Jonathan S. Weissman[3,4,5] ✉ and Britt Adamson[8,9] ✉

Single-cell CRISPR screens enable the exploration of mammalian gene function and genetic regulatory networks. However, use of this technology has been limited by reliance on indirect indexing of single-guide RNAs (sgRNAs). Here we present direct-capture Perturb-seq, a versatile screening approach in which expressed sgRNAs are sequenced alongside single-cell transcriptomes. Direct-capture Perturb-seq enables detection of multiple distinct sgRNA sequences from individual cells and thus allows pooled single-cell CRISPR screens to be easily paired with combinatorial perturbation libraries that contain dual-guide expression vectors. We demonstrate the utility of this approach for high-throughput investigations of genetic interactions and, leveraging this ability, dissect epistatic interactions between cholesterol biogenesis and DNA repair. Using direct capture Perturb-seq, we also show that targeting individual genes with multiple sgRNAs per cell improves efficacy of CRISPR interference and activation, facilitating the use of compact, highly active CRISPR libraries for single-cell screens. Last, we show that hybridization-based target enrichment permits sensitive, specific sequencing of informative transcripts from single-cell RNA-seq experiments.

CRISPR-based genetic tools have recently been paired with high-resolution phenotypic profiling to enable genetic screens with information-rich readouts[1–3]. These efforts have dramatically expanded our ability to investigate genetic control over complex cellular processes. One such approach, independently implemented as Perturb-seq[4,5], CRISP-seq[6], Mosaic-seq[7] and CROP-seq[8] and herein referred to as single-cell CRISPR screening, combines pooled CRISPR screens with single-cell RNA-sequencing (scRNA-seq) to facilitate unbiased exploration of gene function and systematic delineation of genetic regulatory networks. However, current implementations face technical and practical limitations that unnecessarily restrict their use. Here we present advances that address several of these limitations, specifically poor scalability, dependence on specialized vector systems and high cost[9–12], and, by doing so, enable facile and scalable single-cell analysis of both single and combinatorial genetic perturbations. In particular, we establish a strategy for performing single-cell CRISPR screens with programmed pairs of CRISPR sgRNAs, thus facilitating efforts to study redundant gene isoforms or paralogs, investigate *cis*-regulatory genome architecture[13], interrogate gene knockouts while evading rescue[14], phenotype precise genetic edits[15,16] or map genetic interactions (GIs)[17] with scRNA-seq.

The technological crux of all single-cell CRISPR screens is the assignment of perturbation identities to single-cell phenotypes. To achieve this, scRNA-seq-based screening efforts have typically relied on polyadenylated indices, which, unlike nonpolyadenylated sgRNAs, can be recorded on scRNA-seq platforms that capture only polyadenylated RNAs (Supplementary Fig. 1a,b). However, recombination of indexed sgRNA libraries during lentiviral delivery can uncouple indices from their assigned sgRNAs[9–12]. This means that such platforms are limited to arrayed use and restricted scale[9,11]. Notably, one method, CROP-seq, has minimized this problem[8]. CROP-seq uses a clever vector system to deliver sgRNAs to cells. This vector duplicates the sequence of a single encoded sgRNA during lentiviral transduction to produce two expression cassettes on the same construct: one that expresses a functional sgRNA and another that expresses a polyadenylated transcript carrying the sgRNA sequence at the 3′ end. In this way, CROP-seq ensures delivery of pooled guide libraries to cells with faithful pairing of sgRNAs and polyadenylated 'indices'. However, due to constraints on cassette size, CROP-seq is thought to be incompatible with delivery of multiple sgRNAs.

To establish tools for more versatile single-cell CRISPR screens, we sought to directly sequence sgRNAs alongside single-cell transcriptomes. We refer to this approach, which we demonstrate here with droplet-based scRNA-seq, as 'direct-capture Perturb-seq'. As with other methods, droplet-based scRNA-seq uses molecular barcoding to identify transcripts from individual cells. This barcoding occurs during reverse transcription (RT), when both unique molecular identifiers (UMIs) and cell barcodes (CBCs) are added to the 3′ or 5′ ends of messenger RNA sequences (Supplementary Fig. 1a,b)[18–20]. For direct-capture Perturb-seq, we extended this barcoding to nonpolyadenylated sgRNAs by addition of guide-specific primers during RT (Fig. 1a,b). To maximize flexibility, we designed platforms for direct capture with both 5′ and 3′ scRNA-seq. For 5′ scRNA-seq, this required the simple addition of an

[1]Medical Scientist Training Program, University of California, San Francisco, San Francisco, CA, USA. [2]Tetrad Graduate Program, University of California, San Francisco, San Francisco, CA, USA. [3]Department of Cellular and Molecular Pharmacology, University of California, San Francisco, San Francisco, CA, USA. [4]Howard Hughes Medical Institute, University of California, San Francisco, San Francisco, CA, USA. [5]California Institute for Quantitative Biomedical Research, University of California, San Francisco, San Francisco, CA, USA. [6]Department of Microbiology and Immunology, University of California, San Francisco, San Francisco, CA, USA. [7]10x Genomics Inc., Pleasanton, CA, USA. [8]Lewis-Sigler Institute for Integrative Genomics, Princeton University, Princeton, NJ, USA. [9]Department of Molecular Biology, Princeton University, Princeton, NJ, USA. [10]Present address: Program for Computational and Systems Biology, Sloan Kettering Institute, Memorial Sloan Kettering Cancer Center, New York, NY, USA. ✉e-mail: jonathan.weissman@ucsf.edu; badamson@princeton.edu

unbarcoded, guide-specific RT primer to standard protocols (Fig. 1a and Supplementary Fig. 1b), an approach also reported by Mimitou et al. while this work was under review[21]. For 3′ scRNA-seq, the RT configuration necessitated that we implement an entirely new scRNA-seq platform (Fig. 1b). This platform concurrently delivers target-specific, barcoded primers to single-cell reactions alongside barcoded oligo-dT (Fig. 1b and Supplementary Fig. 1a). These target-specific primers anneal to capture sequences (cs1 and cs2) in modified sgRNA constant regions and thus enable RT of sgRNAs and efficient recording of sgRNA sequences (Supplementary Fig. 1c–f, Supplementary Note 1 and Supplementary Table 1). Critically, we selected the capture sequences for our platform carefully. For example, we tested their incorporation into an optimized sgRNA constant region (CR1) to ensure that they would not compromise guide activity. Moreover, we chose capture sequences that are not guide-specific, and thus, in principle, will enable multiplexed capture of additional features, such as antibodies[22,23] and other oligo-tagged markers[24]. Here we refer to guides with cs1 incorporated in a stem loop of our standard *Streptococcus pyogenes* Cas9 sgRNAs (sgRNA-CR1) as sgRNA-CR1^{cs1} and guides with cs2 incorporated at the 3′ end as sgRNA-CR1^{cs2}. We note that an alternate configuration with incorporation of cs1 at the 3′ end compromises activity and therefore is not recommended (Supplementary Fig. 1f).

To test the performance of guide capture, we next performed five parallel CRISPR interference- (CRISPRi)-based[25,26] screens in K562 cells designed these screens to compare 3′ direct capture and 5′ direct capture to indexing by a polyadenylated barcode, which we hereafter refer to as a GBC (guide barcode) Perturb-seq. On each platform, we screened one or more sgRNA libraries containing the same 32 targeting sequences. These sequences target 30 genes whose depletion leads to activation of the unfolded protein response (UPR)[4] and include two nontargeting controls[4]) (Supplementary Table 2). To enable comparison, we prepared each of these libraries using arrayed cloning and lentiviral packaging, and after performing our screens, used custom protocols to amplify index molecules (GBCs or guides) for deep sequencing alongside mRNA sequences (Supplementary Fig. 1g and Supplementary Notes 2 and 3; see Methods). At a constant sequencing depth, screens using both direct-capture platforms gave higher index capture than the GBC-based method (4.1-fold higher for 3′ sgRNA-CR1^{cs1} capture; 15.5-fold higher for 5′ sgRNA-CR1^{cs1} capture; 7.8-fold higher for 5′ sgRNA-CR1 capture), with the exception of 3′ capture of sgRNA-CR1^{cs2}, which had modestly lower capture (0.56-fold) (Supplementary Fig. 2a). To assign guide identities to cells, we then fit a two-component Poisson–Gaussian mixture model to the $\log_2$-transformed guide UMIs per cell for each guide (Supplementary Fig. 2b; see Methods). This approach aims to separate true guide-expressing cells from 'background cells', which arise from spurious cell barcode-sgRNA pairing (potentially due to PCR chimeras or capture of ambient guides). Unlike capture of GBCs, we found that guide capture was targeting sequence-dependent with capture rates varying across guides (Fig. 1c and Supplementary Fig. 2c). This variation was correlated across screens and was related to the nucleotides at the 5′ ends of guide RNAs but not to overall GC content (Supplementary Fig. 2d–g). Nevertheless, our assignment procedure robustly assigned guide identities to 84–94% of cells (compared to 89% for GBC Perturb-seq) with roughly expected guide distributions across all platforms (Fig. 1d and Supplementary Fig. 2h). Moreover, indicative of robust assignment, we found strong (and comparable) target depletion across platforms (median knockdown: 90% for GBC capture, 94% for 3′ sgRNA-CR1^{cs1} capture, 93% for 3′ sgRNA-CR1^{cs2} capture, 95% for 5′ sgRNA-CR1 capture and 93% for 5′ sgRNA-CR1^{cs1} capture) (Supplementary Fig. 3a).

We then sought to benchmark the performance of direct-capture Perturb-seq for the study of genes and genetic networks. High-content Perturb-seq phenotypes should enable (1) functional clustering of target genes, (2) identification of transcriptional phenotypes caused by individual perturbations, (3) delineation of gene expression regulons and (4) identification of cell-to-cell heterogeneities. We therefore asked how phenotypes from our direct capture screens with the highest guide assignment rates (3′ capture of sgRNA-CR1^{cs1} and 5′ capture of sgRNA-CR1) performed on each of these tasks (compared to GBC Perturb-seq). First, we hierarchically clustered target genes based on their pseudo-bulk expression profiles (Fig. 1e). This recapitulated known functional and physical interactions and, when compared to results generated with GBC Perturb-seq, produced highly similar relationships (cophenetic correlation with GBC Perturb-seq: $r=0.95$ for 3′ sgRNA-CR1^{cs1}; $r=0.95$ for 5′ sgRNA-CR1). Next, we evaluated transcriptional responses and found good agreement across platforms (for the top 100 differentially expressed genes, $r=0.88$ for 3′ sgRNA-CR1^{cs1} capture compared to GBC Perturb-seq and $r=0.87$ for 5′ sgRNA-CR1 capture compared to GBC Perturb-seq) with especially high correlations for perturbations that led to differential expression of >100 genes (Supplementary Fig. 3b,c). These results confirm our ability to accurately assign guide identities and suggests that our target-specific RT primers do not globally alter single-cell gene expression profiles. Next, we tested the use of direct-capture Perturb-seq for the discovery of genetic networks. For this, we relied on our previous empirical classification of genes regulated by the three separate signaling branches of the UPR[4]. Examining the covariance of these genes across single cells in our current data, we delineated gene expression modules that were conserved across platforms (cophenetic correlation with GBC Perturb-seq: $r=0.93$ for 3′ sgRNA-CR1^{cs1} capture; $r=0.95$ for 5′ sgRNA-CR1 capture), with modules tending to cluster functionally based on their regulation by the three UPR branches (Fig. 1f). Last, we evaluated the single-cell

Fig. 1 | Design and validation of direct-capture Perturb-seq for 3′ and 5′ single-cell RNA-sequencing. a, Schematic of sgRNA capture during 5′ scRNA-seq. An sgRNA containing a standard constant region (top) anneals to a guide-specific RT oligo. Indexing of reverse transcribed complementary DNA (bottom) occurs after template switch. This strategy is compatible with unmodified sgRNAs (shown) or with sgRNAs with an integrated capture sequence. **b**, Schematic of sgRNA capture via an integrated capture sequence by 3′ scRNA-seq. A capture sequence within the constant region of the sgRNA (top) anneals to a barcoded, target-specific RT primer. Indexed cDNA (bottom) is produced by RT. **c**, Index (GBC or guide) capture rates per cell across experiments conducted with GBC Perturb-seq and direct-capture Perturb-seq. Data represent median index UMI counts per cell for cells bearing each of $n=32$ sgRNAs across platforms. Gray lines indicate median values. 'sgRNA-CR1' indicates standard sgRNAs without a capture sequence. **d**, Index (GBC or guide) assignment rates across experiments conducted with GBC Perturb-seq and direct-capture Perturb-seq. The total number of cells per experiment as well as the fractions of cells assigned no guide, a single guide or more than one guide are indicated. 'sgRNA-CR1' indicates standard sgRNAs without a capture sequence. **e**, Clustering of perturbations from UPR Perturb-seq experiments conducted with GBC Perturb-seq and direct-capture Perturb-seq. Heatmaps represent Spearman's rank correlations between pseudo-bulk expression profiles for each of $n=32$ perturbations. For visual comparison, the rows and columns of all three heatmaps are ordered identically based on the hierarchical clustering of GBC Perturb-seq data. Functional annotations are indicated. **f**, Hierarchical clustering of UPR-regulated genes based on coexpression in each of the indicated Perturb-seq experiments. Colors indicate membership in different UPR-regulated groups as determined by Adamson et al.[4]. **g**, Single-cell projections are based on t-sne visualization of ten independent components ($n=1{,}795$ cells for 3′ GBC Perturb-seq, $n=1{,}595$ cells for 3′ sgRNA-CR1^{cs1} Perturb-seq and $n=1{,}424$ cells for 5′ sgRNA-CR1 Perturb-seq). Colors indicate functional similarities among targeted genes.

performance of our platforms (Fig. 1g). To do this quantitatively, we trained a random forest classifier to classify perturbed and unperturbed (control) cells for each targeting guide. Despite the intrinsic noise of scRNA-seq data, prediction accuracies were highly similar across platforms (correlation with GBC Perturb-seq: $r = 0.91$ for 3′ sgRNA-CR1^{cs1} capture, $r = 0.90$ for 5′ sgRNA-CR1 capture) (Supplementary Fig. 3d).

To demonstrate the versatility of direct-capture Perturb-seq, we next performed a 3′ direct-capture Perturb-seq experiment in induced pluripotent stem cells (iPSCs), now using Cas9 (ref. [27]) and pooled lentiviral packaging and transduction of 40 sgRNAs (Supplementary Table 3). In iPSCs, we again found high guide capture rates (mean capture of 999 UMIs per cell; Supplementary Fig. 4a,b) and transcriptional phenotypes that were correlated for guides targeting the same gene (Supplementary Fig. 4c,d).

Recently, we showed that GBC Perturb-seq can be coupled with epistasis analysis to provide mechanistic insights into how genes interact[17]. However, GBC Perturb-seq is not easily scalable.

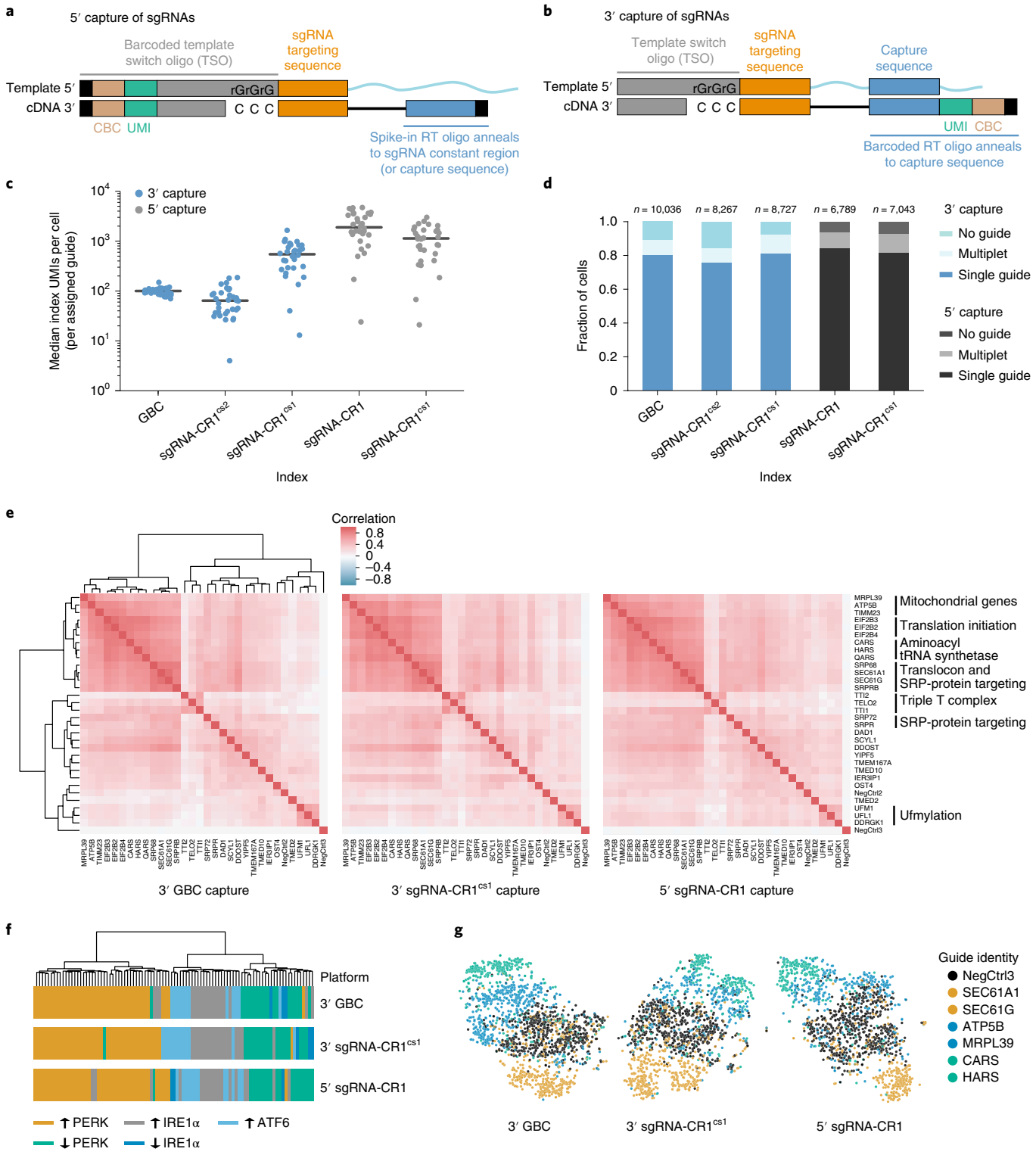

Motivated by this limitation, we next explored the use of direct-capture Perturb-seq to study GIs, specifically a complex set of GIs we recently identified between genes that control cholesterol biosynthesis (for example, *FDPS*, *MVD* and *IDI1*) and genes that facilitate DNA repair (for example, *ATR* and genes encoding components of the 9-1-1 complex)[28]. For this, we cloned a CRISPRi library of 92 programmed sgRNA pairs (targeting 41 genes and 81 gene pairs) using a strategy for pooled cloning of dual-guide vectors (Fig. 2a, Supplementary Fig. 5a and Supplementary Note 4). Notably, we made and tested this library in two configurations using two combinations of guide constant region sequences ($CR3^{cs1}/CR1^{cs1}$ and $CR2^{cs2}/CR1^{cs1}$) (Supplementary Notes 1 and 4 and Supplementary Table 4). Screening this library in K562 cells by 3′ direct-capture Perturb-seq revealed adequate capture of guides from both vector positions (position A, median of 776 UMIs per cell; position B, median of 511 UMIs per cell; Supplementary Fig. 5b,c), and after mapping these guides to cells, we observed >90% guide assignment with >67% of guide-bearing cells expressing two sgRNAs, as expected given multiple infections, doublets from cell loading and imperfect guide calling (Fig. 2b; see Methods). Consistent with similar dual-guide expression systems[4,17,28], we also observed comparable knockdown between the two positions in our dual-guide vector. Specifically, for three guides in our library that were encoded in both positions paired with a nontargeting guide, we achieved target knockdown of 84 and 84% (position A and position B), 81 and 73% (position A and position B) and 70 and 74% (position A and position B). These guides target *HUS1*, *FDPS* and *TOPBP1*, respectively. Of note, the design of our dual-guide expression system minimizes intramolecular recombination between linked sgRNA sequences by using distinct U6 promoters and sgRNA constant regions, as we previously demonstrated[4]; however, it does not prevent paired sgRNA pairs from shuffling due to intermolecular recombination events. Nevertheless, because direct capture allows us to assign sgRNAs to cells in an unbiased way, we were able to identify novel sgRNA pairs and excluded them from downstream analysis.

We previously proposed a model for GIs between cholesterol biosynthesis and DNA repair genes wherein repression of the former leads to the buildup of toxic metabolic intermediates in cells, which then cause replicative stress and replication checkpoint-activated cell-cycle arrest[28]. This model emerged from a set of low-content and low-throughput biochemical and functional experiments that primarily investigated the relationship between key pathway genes, including *FDPS* and a key mediator of the replication checkpoint machinery, *HUS1*. By contrast, direct-capture Perturb-seq allows simultaneous interrogation of many single and double genetic perturbations with information-rich phenotypes. This approach therefore enabled us to thoroughly examine how cells respond to depletion of several enzymes in the cholesterol biosynthesis pathway (Fig. 2c). From this, we made three clear observations. First, as expected, perturbation of early pathway steps led to feedback marked by upregulation of cholesterol biosynthesis genes (Fig. 2d). Second, repression of intermediate pathway genes (*FDPS*, *MVD* and *IDI1*), which are synthetic lethal with DNA repair genes, led to an accumulation of cells in S-phase of the cell cycle (Fig. 2d). Notably, the difference in phenotypes among genes within this linear biosynthetic pathway supports the idea that buildup of toxic intermediates, rather than depletion of cholesterol itself, leads to S-phase arrest. Last, as predicted by our model, we observed a buffering relationship between genes that regulate the early and intermediate steps in cholesterol biosynthesis. Specifically, when we fit a regression model to decompose dual-gene perturbations into linear combinations of single-gene effects, we observed that *PMVK* repression suppressed the *FDPS*-specific transcriptional response, while maintaining the cholesterol feedback response shared by perturbation of both genes (Fig. 2e). This further suggests that S-phase arrest is caused by loss of the enzymatic activity of the intermediate genes, not from a loss of cholesterol itself.

While repression of *HUS1* causes modest cell-cycle aberration alone, in combination with *FDPS* knockdown, we observed a substantial bypass of the S-phase checkpoint and an accumulation of cells in G2/M (Fig. 2f and Supplementary Fig. 5d). Additionally, we found that these cells (with perturbation of both *HUS1* and *FDPS*) demonstrate a neomorphic phenotype characterized by a transcriptional response not induced by either perturbation alone (Fig. 2g). At the single-cell level, this generated a population of G2/M-arrested cells with notably decreased total mRNA content, likely representing dying cells (Fig. 2h). Based on this, we propose an updated model where synthetic lethality in these cells is caused specifically by failure to detect replication stress in HUS1-depleted cells, resulting in inappropriate cell-cycle progression and cell death owing to unresolved damage, potentially by mitotic catastrophe. Broadly, this example highlights the power of high-resolution, single-cell phenotypes for the mechanistic dissection of GIs and

Fig. 2 | Direct-capture Perturb-seq and pooled dual-guide cloning allows systematic dissection of GIs between cholesterol biosynthesis and DNA repair genes. a, Schematic of programmed dual-guide library cloning strategy. Paired sgRNA targeting sequences are synthesized on single oligos and cloned into a direct-capture Perturb-seq vector by ligation. Then, an sgRNA constant region and hU6 promoter are inserted between the sgRNA targeting sequences to generate the final vector. This example shows a $CR3^{cs1}/CR1^{cs1}$ library design. **b**, Guide assignment rates for dual-guide direct-capture Perturb-seq experiments. The fraction of cells carrying sgRNAs (marked by BFP) varied due to strong CRISPRi growth defects; the total number of cells were therefore first scaled by BFP positivity. The total number of cells and fraction of cells assigned a single guide, two guides or more than two guides are indicated. **c**, Schematic of the cholesterol biosynthesis pathway. **d**, Heatmap of cell cycle and cholesterol phenotypes for cells with CRISPRi-based perturbations of the cholesterol biosynthesis pathway. Cell-cycle occupancy indicates the relative enrichment or depletion of cells in each phase relative to unperturbed cells. The cholesterol score is the mean *z*-scored expression of enzymes in the cholesterol biosynthesis pathway. The 'HUS1 GI' is a metric of the growth defect caused by the indicated perturbations paired with *HUS1* knockdown relative to individual phenotypes, as determined by Horlbeck et al.[28]. Percentage knockdown: *HMGCR* 94%; *PMVK* 92%; *MVD* 83%; *FDPS* 78%; *IDI1* 82% and *SQLE* 84%). Number of cells per perturbation (expressed from a dual-guide vector paired with a nontargeting control): nontargeting control $n=527$, HMGCR $n=608$, PMVK $n=389$, MVD $n=184$, FDPS $n=439$, IDI1 $n=131$ and SQLE $n=255$. **e**, Heatmap of gene expression for the 50 most differentially expressed genes among cells carrying each indicated perturbation. Expression values are the *z*-scored expression relative to unperturbed cells ($n=389$ PMVK cells, $n=1{,}921$ FDPS cells and $n=517$ PMVK/FDPS cells). Cells were combined to generate the expression signatures. Knockdown was consistent between single-gene and dual-gene targeting (*FDPS* knockdown 73% alone versus 82% paired; *PMVK* knockdown 92% alone versus 86% paired). The indicated GI score was previously determined by Horlbeck et al.[28], where GI scores >3 are considered strongly buffering interactions. **f**, Fraction of cells in each cell-cycle phase across cells with the indicated perturbations. Number of cells per perturbation: nontargeting control $n=780$, HUS1 $n=905$, FDPS $n=439$ and HUS1/FDPS $n=831$. **g**, Heatmap of gene expression for the 50 most differentially expressed genes among cells carrying each indicated perturbation. Expression values are the *z*-scored expression relative to unperturbed cells ($n=905$ HUS1 cells, $n=439$ FDPS cells and $n=831$ HUS1/FDPS cells). Cells were combined to generate the expression signatures. Knockdown was consistent between single-gene and dual-gene targeting (*FDPS* knockdown 78% alone versus 72% paired; *HUS1* knockdown 95% alone versus 85% paired). The indicated GI score was previously determined by Horlbeck et al.[28], where GI scores <−3 are considered strongly synergistic interactions. **h**, Single-cell uniform manifold approximation and projections with informative cell features highlighted ($n=2{,}175$ cells).

demonstrates how direct-capture Perturb-seq can be used to understand GIs in a comprehensive, unbiased fashion without the need for specific hypotheses.

To further enable single-cell CRISPR screening efforts, we next tested the idea that co-delivery of multiple sgRNAs per gene to the same cell could increase screening efficiency by allowing the use

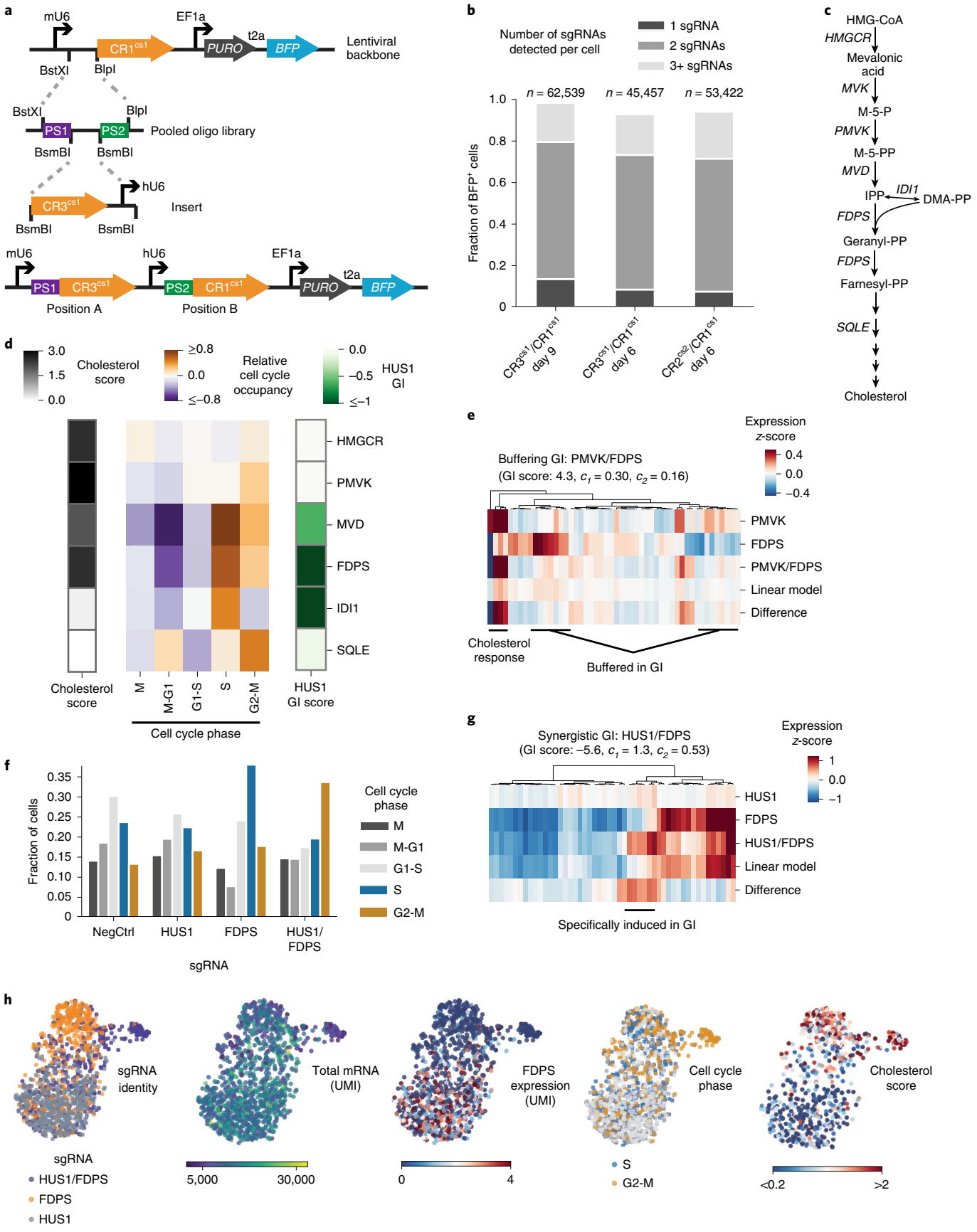

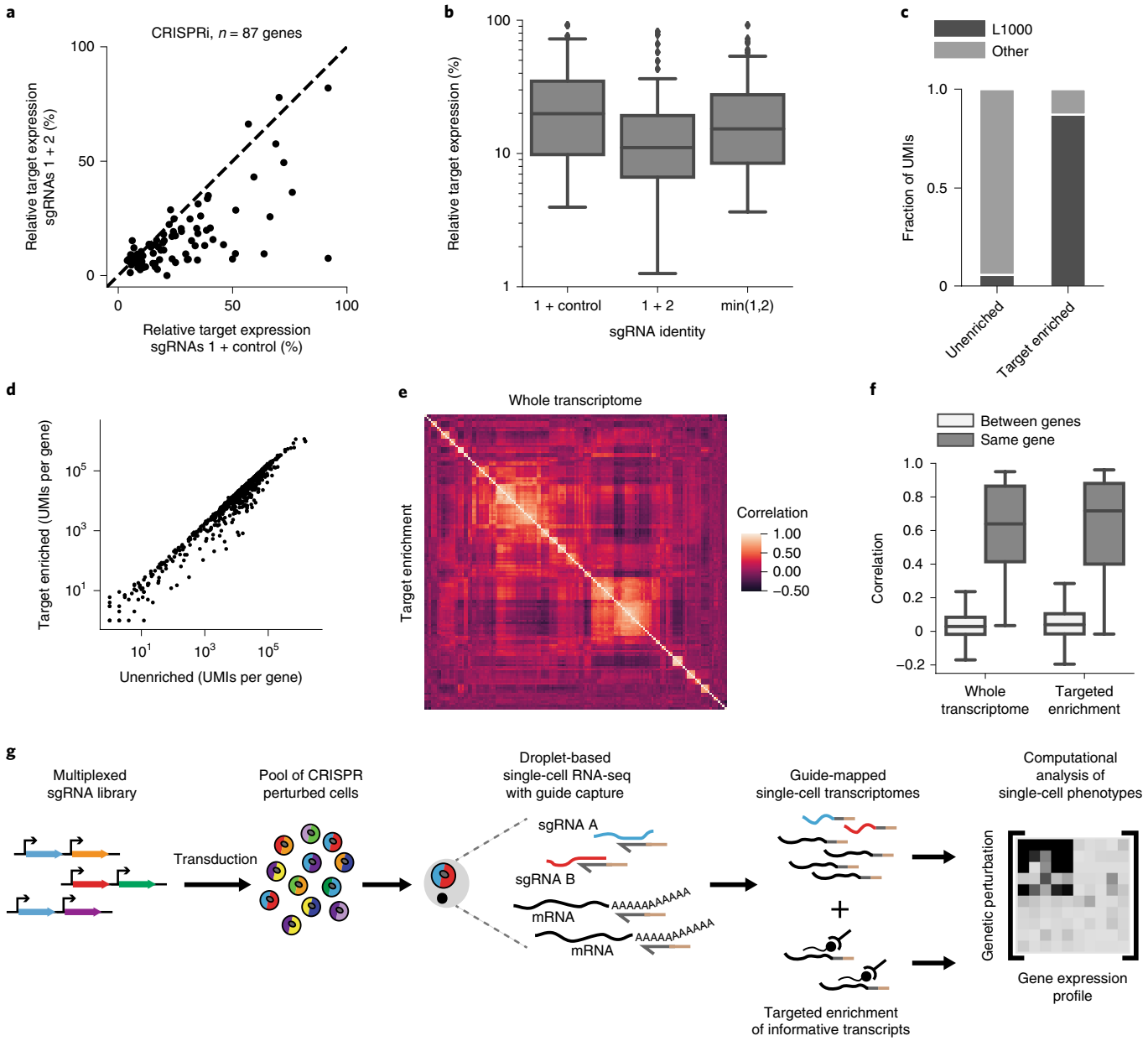

Fig. 3 | Multiplexed CRISPRi/CRISPRa and hybridization-based target enrichment to enable scalable and versatile single-cell CRISPR screens. **a**, Scatterplot of the relative target expression per gene comparing CRISPRi knockdown with a single sgRNA (expressed from a dual-guide vector paired with a nontargeting control) versus multiplexed sgRNAs. Multiplexed sgRNAs significantly improve knockdown (sgRNAs 1+control median relative target expression, 0.20; sgRNAs 1+2 median relative target expression, 0.11; Wilcoxon signed-rank two-sided test $n=87$ genes, $W=378$, $P=8\times10^{-11}$). sgRNA 1, best predicted sgRNA for each gene. sgRNA 2, second best predicted sgRNA for each gene. **b**, Box plots of the relative target expression per gene in the multiplexed CRISPRi experiment denoting quartile ranges (box), median (center mark) and 1.5× interquartile range (whiskers). 'min(1,2)' indicates the minimum remaining target expression between sgRNA 1 (paired with negative control) and sgRNA 2 (paired with negative control); that is, the predicted multiplexed sgRNA knockdown based on a dominant model of knockdown. The multiplexed sgRNAs performed better than the dominant model (Wilcoxon signed-rank two-sided test $n=87$ genes, $W=698$, $P=3\times10^{-7}$). **c**, The fraction of total UMIs for L1000 genes ($n=978$) versus other genes from K562 cells, before and after target enrichment. **d**, Scatterplot of the total number of UMIs for each gene, before and after target enrichment ($n=978$ genes). The Pearson correlation of $\log_{10}$ normalized UMIs is $r=0.98$. **e**, Heatmap depicts clustering of guides in our multiplexed CRISPRi experiment. Heatmap represents Spearman's rank correlations between pseudo-bulk expression profiles of well-expressed genes (>1 UMIs per cell). Data from all perturbations with more than ten differentially expressed genes compared to controls are included ($n=145$ genes). The upper triangle (correlation matrix) was calculated on the whole transcriptome while the lower triangle (correlation matrix) was calculated on the target-enriched transcriptome. Both triangles were identically ordered based on hierarchical clustering of the whole transcriptome correlation matrix. **f**, Pearson correlations of pseudo-bulk differential expression profiles of well-expressed genes (>1 UMIs per cell) caused by sgRNAs targeting the same gene (for $n=39$ genes whose knockdown led to differential gene expression) versus sgRNAs targeting different genes ($n=111{,}592$ pairs). sgRNAs targeting the same gene had significantly more similar profiles than sgRNAs targeting different genes, both before and after target enrichment (unenriched median $r=0.64$, Mann–Whitney U two-sided test $U=117{,}224$, $P=1.4\times10^{-24}$; enriched median $r=0.72$, Mann–Whitney U two-sided test $U=259{,}898$, $P=1.7\times10^{-21}$). Box plots denote quartile ranges (box), median (center mark) and 1.5× interquartile range (whiskers). **g**, Schematic overview of direct-capture Perturb-seq workflow.

of libraries with fewer constructs per gene. To test this, we selected pairs of CRISPRi and CRISPR activation (CRISPRa) sgRNAs with high predicted activity[29] against individual genes (87 for CRISPRi, 49 for CRISPRa; Supplementary Tables 5 and 6). These genes span a range of biological functions and expression levels. Then, using our pooled library cloning strategy and direct-capture Perturb-seq in K562 cells, we compared the activity (knockdown or activation) of guide pairs expressed from one vector to single sgRNAs (expressed from the same dual-guide vector paired with nontargeting control sgRNAs). For both CRISPRi and CRISPRa, the multiplexed sgRNAs nearly doubled CRISPR activity over what was achieved with the best single guide (CRISPRi: sgRNAs 1 + control, median relative target expression, 0.20; sgRNAs 1 + 2, median relative target expression, 0.11; Wilcoxon signed-rank two-sided test $n = 87$ genes, $W = 378$, $P = 8 \times 10^{-11}$; CRISPRa: sgRNAs 1 + control, median fold-activation, 2.9; sgRNAs 1 + 2, median fold-activation, 4.7; Wilcoxon signed-rank two-sided test $n = 49$ genes, $W = 162$, $P = 7 \times 10^{-6}$; Fig. 3a,b and Supplementary Fig. 6a,b). Moreover, in both cases, the multiplexed sgRNAs appeared to perform better than expected based on a dominant model of guide activity, suggesting some degree of synergy between multiplexed sgRNAs (CRISPRi Wilcoxon signed-rank two-sided test: $n = 87$ genes, $W = 698$, $P = 3 \times 10^{-7}$; CRISPRa Wilcoxon signed-rank two-sided test: $n = 49$ genes, $W = 233$, $P = 0.0002$; Supplementary Fig. 6c–f), which is consistent with previous reports[30,31]. These results show that compact, highly active libraries (expressing multiple sgRNAs per gene) can be used to scale single-cell experiments with direct-capture Perturb-seq, interrogating more genes while minimizing false negatives due to insufficient expression modulation.

Last, we addressed the fact that current implementations of scRNA-seq are constrained by sequencing the whole transcriptome for phenotyping, which can be prohibitively expensive. This requirement is compounded by the fact that the distribution of gene expression is skewed (that is, 2% of expressed genes consume >50% of sequencing reads; Supplementary Fig. 7a) and biased across gene functions. Indeed, genes with important biological functions (for example, transcription factors, cell-surface receptors, kinases) are often lowly expressed and difficult to measure (Supplementary Fig. 7b). However, given a suitable method for targeted enrichment of scRNA-seq libraries, many transcriptional states could be faithfully inferred from a subset of gene expression measurements[32,33]. Diverse approaches exist for enriching transcripts using multiplexed PCR[34], custom RT beads[35] or linear amplification[36]; however, each of these is limited by number of target genes, quality and/or a priori gene selection. Instead, we hypothesized that we could use hybridization-based target enrichment to specifically sequence thousands of select transcripts, thereby limiting sequencing while maintaining high-content phenotypes.

To test target enrichment, we empirically designed hybridization baits for 978 genes, the L1000 landmark genes[33] (Supplementary Note 5 and Supplementary Table 7). We chose these genes because they can serve as a reduced representation of the whole transcriptome and their expression levels span four orders of magnitude, providing ample range to examine potential biases introduced by hybridization capture. In our test, we performed a pulldown on a 3′ scRNA-seq library from K562 cells and deeply sequenced recovered molecules. Hybridization capture increased the percentage of mRNA molecules aligning to target genes by >14-fold, from 6% in an unenriched control to 87% after target enrichment (Fig. 3c). Thus, at only ~0.1× sequencing depth of the original library, the enriched library contains more UMIs per cell for most targeted genes (Supplementary Fig. 7c). Enriched gene expression profiles were highly correlated with unenriched profiles at the global ($r = 0.98$), single-cell (median $r = 0.93$) and single-gene (median $r = 0.75$) levels (Fig. 3d, Supplementary Fig. 7d–f and Supplementary Note 6), and perturbation-dependent differential gene expression was highly similar before and after enrichment (median $r = 0.71$; Supplementary Fig. 7g). Given these results, we next tested the ability of our reduced transcriptome subset to functionally cluster genes. Hybridization capture on our multiplexed CRISPRi Perturb-seq libraries revealed that L1000-targeted gene expression profiles can recapitulate relationships between genetic perturbations established by sequencing the entire transcriptome (cophenetic correlation $r = 0.95$; Fig. 3e,f and Supplementary Fig. 7h). Altogether, these results demonstrate that hybridization capture is a simple and sensitive procedure for informative enrichment of tailored gene sets from scRNA-seq libraries. Moreover, because our target enrichment procedure is performed on final libraries, target genes do not need to be selected a priori and can be iteratively refined for a single experiment. This technology motivates the future optimization of gene sets that maximize biological information while minimizing sequencing requirements (analogous to the L1000 landmark genes for hybridization-based fluorescent assays[33]).

Since its inception, single-cell CRISPR screening has made it possible to simultaneously examine high-dimensional genotypic and phenotypic landscapes. Here we described several improvements to Perturb-seq that substantially expand the scale and flexibility of this technology (Fig. 3g and Supplementary Table 8). Our 5′ and 3′ direct-capture Perturb-seq platforms (now commercially available from 10x Genomics) have crucial advantages under different circumstances. For example, 5′ direct capture is compatible with standard sgRNAs, has higher guide capture rates, and allows for V(D)J clonotype analysis, whereas 3′ direct capture is compatible with many molecular recording and lineage tracing approaches[37]. We specifically demonstrated the value of direct capture for the mechanistic dissection of GIs, which is a laborious undertaking with other methods, and for generating compact, highly active CRISPR libraries. Additionally, to decrease the cost of Perturb-seq experiments, we implemented hybridization-based target enrichment. With our target enrichment strategy, biologically meaningful gene panels (for example, immune, developmental, metabolic, tumor suppressors/oncogenes and so on) can be probed without unnecessary sequencing of housekeeping genes. Taken together, direct-capture Perturb-seq and target enrichment greatly expand the accessibility, scalability and flexibility of single-cell CRISPR screens.

Online content

Any methods, additional references, Nature Research reporting summaries, source data, extended data, supplementary information, acknowledgements, peer review information; details of author contributions and competing interests; and statements of data and code availability are available at https://doi.org/10.1038/s41587-020-0470-y.

Received: 20 December 2018; Accepted: 26 February 2020;
Published online: 30 March 2020

References

1. Packer, J. & Trapnell, C. Single-cell multi-omics: an engine for new quantitative models of gene regulation. *Trends Genet.* **34**, 653–665 (2018).
2. Feldman, D. et al. Optical pooled screens in human cells. *Cell.* **179**, 787–799.e17 (2019).
3. Rubin, A. J. et al. Coupled single-cell CRISPR screening and epigenomic profiling reveals causal gene regulatory networks. *Cell.* **176**, 361–376.e17 (2018).
4. Adamson, B. et al. A multiplexed single-cell CRISPR screening platform enables systematic dissection of the unfolded protein response. *Cell.* **167**, 1867–1882.e21 (2016).
5. Dixit, A. et al. Perturb-Seq: dissecting molecular circuits with scalable single-cell RNA profiling of pooled genetic screens. *Cell.* **167**, 1853–1866.e17 (2016).
6. Jaitin, D. et al. Dissecting immune circuits by linking CRISPR-pooled screens with single-cell RNA-seq. *Cell.* **167**, 1883–1896.e15 (2016).
7. Xie, S., Duan, J., Li, B., Zhou, P. & Hon, G. C. Multiplexed engineering and analysis of combinatorial enhancer activity in single cells. *Mol. Cell.* **66**, 285–299.e5 (2017).

8. Datlinger, P. et al. Pooled CRISPR screening with single-cell transcriptome readout. *Nat. Methods* **14**, 297–301 (2017).
9. Hill, A. J. et al. On the design of CRISPR-based single-cell molecular screens. *Nat. Methods* **15**, 271 (2018).
10. Adamson, B., Norman, T. M., Jost, M. & Weissman, J. S. Approaches to maximize sgRNA-barcode coupling in Perturb-seq screens. Preprint at *bioRxiv* https://doi.org/10.1101/298349 (2018).
11. Xie, S., Cooley, A., Armendariz, D., Zhou, P. & Hon, G. C. Frequent sgRNA-barcode recombination in single-cell perturbation assays. *PLoS ONE* **13**, e0198635 (2018).
12. Feldman, D., Singh, A., Garrity, A. J. & Blainey, P. C. Lentiviral co-packaging mitigates the effects of intermolecular recombination and multiple integrations in pooled genetic screens. Preprint at *bioRxiv* https://doi.org/10.1101/262121 (2018).
13. Gasperini, M. et al. A genome-wide framework for mapping gene regulation via cellular genetic screens. *Cell.* **176**, 377–390.e19 (2019).
14. Smits, A. H. et al. Biological plasticity rescues target activity in CRISPR knock outs. *Nat. Methods* **16**, 1087–1093 (2019).
15. Anzalone, A. V. et al. Search-and-replace genome editing without double-strand breaks or donor DNA. *Nature* **576**, 149–157 (2019).
16. Ran, A. F. et al. Double nicking by RNA-guided CRISPR Cas9 for enhanced genome editing specificity. *Cell* **154**, 1380–1389 (2013).
17. Norman, T. M. et al. Exploring genetic interaction manifolds constructed from rich single-cell phenotypes. *Science* **365**, 786–793 (2019).
18. Macosko, E. Z. et al. Highly parallel genome-wide expression profiling of individual cells using nanoliter droplets. *Cell* **161**, 1202–1214 (2015).
19. Klein, A. M. et al. Droplet barcoding for single-cell transcriptomics applied to embryonic stem cells. *Cell* **161**, 1187–1201 (2015).
20. Zheng, G. X. et al. Massively parallel digital transcriptional profiling of single cells. *Nat. Commun.* **8**, 14049 (2017).
21. Mimitou, E. P. et al. Multiplexed detection of proteins, transcriptomes, clonotypes and CRISPR perturbations in single cells. *Nat. Methods* **16**, 409–412 (2019).
22. Stoeckius, M. et al. Simultaneous epitope and transcriptome measurement in single cells. *Nat. Methods* **14**, 865–868 (2017).
23. Peterson, V. M. et al. Multiplexed quantification of proteins and transcripts in single cells. *Nat. Biotechnol.* **35**, 936–939 (2017).
24. Zhang, S.-Q. et al. High-throughput determination of the antigen specificities of T cell receptors in single cells. *Nat. Biotechnol.* **36**, 1156–1159 (2018).
25. Gilbert, L. A. et al. Genome-scale CRISPR-mediated control of gene repression and activation. *Cell* **159**, 647–661 (2014).
26. Gilbert, L. A. et al. CRISPR-mediated modular RNA-guided regulation of transcription in eukaryotes. *Cell* **154**, 442–451 (2013).
27. Mandegar, M. A. et al. CRISPR interference efficiently induces specific and reversible gene silencing in human iPSCs. *Cell Stem Cell* **18**, 541–553 (2016).
28. Horlbeck, M. A. et al. Mapping the genetic landscape of human cells. *Cell* **174**, 953–967.e22 (2018).
29. Horlbeck, M. A. et al. Compact and highly active next-generation libraries for CRISPR-mediated gene repression and activation. *eLife* **5**, e19760 (2016).
30. Moreno, A. M. et al. In situ gene therapy via AAV-CRISPR-Cas9-mediated targeted gene regulation. *Mol. Ther.* **26**, 1818–1827 (2018).
31. Savell, K. E. et al. A neuron-optimized CRISPR/dCas9 activation system for robust and specific gene regulation. *eNeuro* **6**, https://doi.org/10.1523/ENEURO.0495-18.2019 (2019).
32. Cleary, B., Cong, L., Cheung, A., Lander, E. S. & Regev, A. Efficient generation of transcriptomic profiles by random composite measurements. *Cell* **171**, 1424–1436.e18 (2017).
33. Subramanian, A. et al. A next generation connectivity map: L1000 platform and the first 1,000,000 profiles. *Cell.* **171**, 1437–1452.e17 (2017).
34. Salomon, R. et al. Droplet-based single cell RNAseq tools: a practical guide. *Lab. Chip* **19**, 1706–1727 (2019).
35. Saikia, M. et al. Simultaneous multiplexed amplicon sequencing and transcriptome profiling in single cells. *Nat. Methods* **16**, 59–62 (2019).
36. Vallejo, A. F. *et al.* Resolving cellular systems by ultra-sensitive and economical single-cell transcriptome filtering. Preprint at *bioRxiv* https://doi.org/10.1101/800631 (2019).
37. Chan, M. M. et al. Molecular recording of mammalian embryogenesis. *Nature* **570**, 77–82 (2019).

Methods

Cell culture and viral production. RPMI-1640 with 25 mM HEPES, 2.0 g l^{-1} NaHCO3, 0.3 g l^{-1} L-glutamine supplemented with 10% FBS, 2 mM glutamine, 100 units per ml penicillin and 100 µg ml^{-1} streptomycin were used to grow K562 cells. Human embryonic kidney (HEK) 293T (HEK293T) cells, used for packaging lentivirus, were grown in Dulbecco's modified eagle medium in 10% FBS, 100 units per ml penicillin and 100 µg ml^{-1} streptomycin. iPSCs expressing Cas9 (WTC CRISPRn Gen1C[27]) were maintained under feeder-free conditions on growth factor-reduced Matrigel (Corning) in mTeSR medium (STEMCELL Technologies). Accutase (STEMCELL Technologies) was used to enzymatically dissociate iPSCs into single cells to passage with 10 µM p160-Rho-associated coiled-coil kinase inhibitor Y-27632 (Selleckchem) added to promote cell survival. Lentivirus was produced by cotransfecting HEK293T cells with transfer plasmids and standard packaging vectors using *Trans*IT-LTI Transfection Reagent (Mirus, MIR 2306).

Plasmid construction and development of sgRNA capture sequences. Guide RNAs were designed for 3′ direct capture Perturb-seq by appending nonrandom capture sequences to the 3′ end of standard guide sequences or by inserting these sequences into the loop region of the so-called 'stem loop 2' (Supplementary Fig. 1c and Supplementary Table 1). Expression vectors encoding these guides are available at Addgene (sgRNA-CR1^{cs1} in pBA904, Addgene #122238; sgRNA-CR1^{cs2} in pBA900, Addgene #122237). To test the activity of modified guides and guide expression vectors (including an optimized CROP-seq vector, pBA950, Addgene #122239), expression constructs carrying green fluorescent protein-(GFP-)targeting guides with variant constant regions were transduced into GFP+K562 dCas9-KRAB cells[4] with centrifugation (2 h at 1,000*g* at 33 °C). Cells were analyzed by flow cytometry on an LSR II flow cytometer (BD Biosciences). Data in Supplementary Fig. 1d were processed as follows: Measurements of median GFP were recorded from GFP+K562 dCas9-KRAB cells transduced with the indicated guides. These measurements were adjusted by subtracting background fluorescence (collected from control cells that do not express GFP) and then divided by measurements of median GFP (also background-subtracted) recorded from cells without a GFP-targeting guide (untransduced cells grown in the same wells). These 'GFP remaining' ratios were then normalized to those derived from cells transduced with a positive control guide, our standard sgRNA-CR1, and are reported as averages of triplicates from separate infections. Data in Supplementary Figs. 1e,f and 5a are shown as the Gaussian kernel density estimates of normalized flow-cytometry measurements representing GFP expression of all cells with the indicated guide RNAs. We chose final guide designs based on GFP depletion results (Supplementary Note 1). The reverse complements of finalized capture sequences (cs1 5′-GCTTTAAGGCCGGTCCTAGCAA-3′ and cs2 5′-GCTCACCTATTAGCGGCTAAGG-3′) were incorporated into gel beads in the Chromium Single-Cell 3′ Reagent Kits v.3 with Feature Barcoding technology.

Pilot UPR direct-capture Perturb-seq. For these experiments, we constructed three CRISPRi libraries (the UPR GBC, UPR sgRNA-CR1^{cs1} and UPR sgRNA-CR1^{cs2} libraries) by arrayed cloning (Supplementary Note 2 and Supplementary Table 2). Each of these libraries encodes guide RNAs programmed with 32 unique guide RNA targeting sequences: 30 that target genes whose depletion was previously shown to activate the UPR by GBC Perturb-seq[4] and two nontargeting controls (sgNegCtrl2 and sgNegCtrl3). Our sequence-verified libraries were then packaged into lentiviruses by arrayed transfection of individual vectors, and lentiviral preparations from each library were pooled for cotransduction into K562 dCas9-KRAB cells[25] (spinfected 2 h at 1,000*g* at 33 °C). To ensure adequate representation of each guide at the time of scRNA-seq (7 d after transduction), lentiviral pooling was performed in a manner that accounted for both packaging variability and guide effects on cell growth after transduction (as determined by individual test infections). Pooling ratios were designed to ensure even representation among targeting guides and delivery of sgNegCtrl2 and sgNegCtrl3 at four-fold excess. Three days post infection, we measured blue fluorescent protein (BFP) expression (a marker for guide transduction) on an LSR II flow cytometer (BD Biosciences) and calculated the percentage of transduced cells for each library (4% for the GBC library, 5% for the sgRNA-CR1^{cs1} library and 5% for the sgRNA-CR1^{cs2} library). Transduced cells were sorted to near purity (FACSAria2, BD Biosciences). Up to this point, cell viability for all three libraries remained >87%.

Seven days post infection, cells were separated into droplet emulsions using the Chromium Controller (10x Genomics) across five lanes (cell pools >94% BFP$^+$). Cells transduced with the UPR GBC library were loaded on two lanes. On one lane, cell capture was performed with Chromium Single-Cell 3′ Gel Beads v2 (GBC Perturb-seq), while on the other, cell capture was performed with Chromium Single-Cell 5′ Gel Beads and a spike-in of 5 pmol of oJR160 (5′-AAGCAGTGGTATCAACGCAGAGTACCAAGTTGATAACGGACTA GCC-3′) to the RT Master Mix (5′ direct-capture Perturb-seq using sgRNA-CR1). Similarly, cells transduced with the UPR sgRNA-CR1^{cs1} library were loaded onto two lanes. On one lane, cell capture was performed with Chromium Single-Cell 3′ Gel Beads v3 (3′ direct-capture Perturb-seq using sgRNA-CR1^{cs1}), while on the other, cell capture was performed with Chromium Single-Cell 5′ Gel Beads and a 5 pmol spike-in of oJR161 (5′-AAGCAGTGGTATCAACGCAGAGTACTTGCTAGGACCGGCCTTAAAGC-3′) to the RT Master Mix (5′ direct-capture Perturb-seq using sgRNA-CR1^{cs1}). Finally, cells transduced with UPR sgRNA-CR1^{cs2} were loaded onto a single lane with Chromium Single-Cell 3′ Gel Beads v3 (3′ direct-capture Perturb-seq using sgRNA-CR1^{cs2}). For all lanes, cells were loaded to recover ~10,000 cells (~260 cells per guide). Approximately 100 pmol of 10x Genomics RT oligo (poly-dT RT Primer PN-2000007) are added to each RT reaction based on quantification by NanoDrop spectrophotometer (Thermo Scientific). Therefore, for 5′ direct-capture Perturb-seq, we chose to add our guide capture oligos at ~5%. The recovered cells and subsamples thereof are analyzed in Fig. 1c–g and Supplementary Figs. 2 and 3.

iPSC 3′ direct-capture Perturb-seq. To test direct-capture Perturb-seq with iPSC cells, we constructed a sequence-verified library of 40 guides using the sgRNA-CR1^{cs1} design by arrayed cloning (Supplementary Note 2 and Supplementary Table 3). This 'iPSC sgRNA-CR1^{cs1}' library was then packaged into lentivirus (pooled format), and transduced into iPSCs carrying inducible Cas9 (ref. [29]) at a percentage of transduced cells of 10%. iPSCs were treated daily with 2 µM doxycycline (Sigma) to drive Cas9 expression and after 2 d, BFP$^+$ cells were enriched on a BD FACSAria2 (BFP is a marker of guide vector transduction). Seven days post infection, cells were separated into droplet emulsions using the Chromium Controller (10x Genomics) with Chromium Single-Cell 3′ Gel Beads v3. The recovered cells and subsamples thereof are analyzed in Supplementary Fig. 4.

Dual-guide 3′ direct-capture Perturb-seq to evaluate GIs. To dissect the interaction between cholesterol biosynthesis and DNA repair, we constructed two sequence-verified dual-guide libraries of manually curated guide pairs by pooled cloning (CR3^{cs1}/CR1^{cs1} and CR2^{cs2}/CR1^{cs1}; Supplementary Note 4 and Supplementary Table 4). Vectors necessary for construction of dual-guide libraries are available at Addgene (pJR85, BsmBI-deleted sgRNA-CR1^{cs1} lentiviral vector, Addgene #140095; pJR89, CR3^{cs1}-hU6 insert, Addgene #140096). For each library, lentivirus was prepared in a pooled format and transduced into K562 dCas9-KRAB cells (spinfection for 2 h at 1,000*g*). Three days post infection, we calculated the percentage of transduced cells (using BFP expression) and sorted transduced cells to near purity (LSR II and FACSAria2, BD Biosciences). To maximize the probability of observing interpretable transcriptional responses, we sampled cells at two time points (day 6 and day 9 post-transduction). At 6 d post infection, we separated cells transduced with CR3^{cs1}/CR1^{cs1} (percentage of transduced cells = 15%, 89% BFP$^+$) and CR2^{cs2}/CR1^{cs1} (percentage of transduced cells = 18%, 93% BFP$^+$) libraries into droplet emulsions using the Chromium Controller with Chromium Single-Cell 3′ Gel Beads v3. At 9 d post infection, we did the same for a second population of cells transduced with the CR3^{cs1}/CR1^{cs1} library (percentage of transduced cells = 10%, 83% BFP$^+$), both times aiming to recover 15,000 cells per lane.

Multiplexed CRISPRi and CRISPRa 3′ direct-capture Perturb-seq. To determine whether guide multiplexing can be used to construct compact CRISPRi and CRISPRa libraries, we built and analyzed dual-guide libraries wherein vectors contain either one targeting guide (paired with a negative control guide) or two guides targeting a single gene (Supplementary Note 4). For these libraries, we manually chose gene targets representing a broad range of biological functions and expression levels (87 for CRISPRi, 49 for CRISPRa). We selected guide RNA targeting sequences predicted to be highly active (the top two by rank in hCRISPRi v.2.1 and hCRISPRa v.2, ref. [30]) (Supplementary Tables 5 and 6). In this manuscript, we refer to guides containing the top ranked targeting sequence as 'sgRNA 1' and the next best as 'sgRNA 2'. Of note, when the selected targeting sequence pairs targeted genomic sequence <80 base pairs (bp) apart, we also included the next best-ranked guide RNA spaced >80 bp away from the first. We refer to guides containing these targeting sequences as 'sgRNA 3'. Additionally, for genes with two annotated transcription start sites, we included the top sgRNAs pairs targeting each transcription start site. We cloned these libraries in pooled format (Supplementary Note 4). We then packaged each library into lentivirus (pooled format) and transduced K562 dCas9-KRAB cells[25] (CRISPRi) and K562 dCas9-SunTag/scFV-VP64 cells[25] (CRISPRa) with the appropriate library. Three days post infection, we calculated percentages of transduced cells (by BFP expression) of 10% and 4.5%, respectively, and sorted transduced cells to near purity (LSR II and FACSAria2, BD Biosciences). Then, 8 d post infection, we separated cells (CRISPRi at 90% BFP+ and CRISPRa at 88% BFP+) into droplet emulsions using the Chromium Controller with Chromium Single-Cell 3′ Gel Beads v3, aiming to recover 15,000 cells per lane.

Sequencing library preparation. Gene expression sequencing libraries from GBC Perturb-seq were prepared according to the Chromium Single-Cell 3′ Reagent Kits v2 User Guide (10x Genomics CG00052) with 11 cycles of PCR during cDNA amplification and 11 cycles of Sample Index PCR. Library molecules containing GBCs were then specifically amplified using KAPA HiFi ReadyMix with 30 ng of the final library as template, 0.6 mM 052-P5 (5′-AATGATACGGCGACCACCGA GATCTACAC-3′) and 0.6 mM of i7 barcoded 055-N708 (5′-CAAGCAGAAGAC-GGCATACGAGATCCTCTCTGGTCTCGTGGGCTCGGAGATGTGTATAAG-AGACAGGACCTCCCTAGCAAACTGGGGCACAAG-3′). PCR cycling was performed according to the following protocol: (1) 95 °C for 3 min, (2) 14 cycles of

98 °C for 15 s, then 70 °C for 10 s and (3) 72 °C for 1 min. The resulting GBC sequencing library was purified via a 0.8× solid-phase reversible immobilization (SPRI) selection (SPRIselect Beckman Coulter #B23318).

Sequencing libraries from 3′ direct-capture Perturb-seq were prepared using a protocol modified from the Chromium Single-Cell 3′ Reagent Kits v3 User Guide (10x Genomics, CG000184) (Supplementary Fig. 1b). This protocol can now be found at https://support.10xgenomics.com/single-cell-gene-expression/library-prep/doc/user-guide-chromium-single-cell-3-reagent-kits-user-guide-v3-chemistry-with-feature-barcoding-technology-for-crispr-screening. Briefly, following 11 cycles of cDNA amplification, library amplicons were size separated into two fractions (Supplementary Fig. 1g): one enriched for amplicons containing guide sequences (by performing a 0.6–1.2× double-sided SPRI), and the other (eluted from the 0.6× left-sided SPRI) containing larger cDNA amplicons. We processed the latter into gene expression sequencing libraries according to the Chromium Single-Cell 3′ Reagent Kits v.3 User Guide (in this case, using ten cycles of Sample Index PCR). In parallel, we used the guide-enriched cDNA amplicons to make perturbation index sequencing libraries. For this, guide-enriched cDNAs amplicons were purified by an additional 1× SPRI selection (30 µl elution). The eluted material (5 µl) was then used as template in the following nested PCR strategy: PCR1 was performed with 50 µl Amp Mix (10x Genomics, PN no. 2000047), 45 µl Feature SI Primers 1 (10x Genomics, PN no. 2000098) and cycling by (1) 98 °C for 45 s, (2) 12 cycles of 98 °C for 20 s, then 60 °C for 5 s, then 72 for 5 s and (3) 72 °C for 1 min. PCR2 was performed with the products of the first PCRs (5 µl after cleanup using a 1× SPRI selection and elution in 30 µl), 50 µl of Amp Mix (10x Genomics, PN no. 2000047), 35 µl of Feature SI Primers 2 (10x Genomics, PN no 2000098) and cycling by (1) 98 °C for 45 s, (2) five cycles of 98 °C for 20 s, then 54 °C for 30 s, then 72 for 20 s and (3) 72 °C for 1 min. Finally, the resulting guide sequencing libraries were cleaned up via a double-sided 0.7–1.0× SPRI selection.

Sequencing libraries from 5′ direct-capture Perturb-seq were prepared using a protocol modified from the Chromium Single-Cell V(D)J Reagent Kits User Guide (10x Genomics CG000086) (Supplementary Fig. 1g and Supplementary Note 3). For this, we used two direct capture spike-in oligos, oJR160 and oJR161, each with an adapter identical to the adapter sequence contained on the Poly-dT RT Primer from 10x Genomics (PN-2000007). This adapter serves as a primer binding site for the NonPoly(dT) primer (10x Genomics, PN-220106) during cDNA amplification, and thus allows amplification of reverse transcribed guides to occur concurrently with standard cDNA amplification. Following 11 cycles of amplification, cDNA amplicons were size separated into two fractions as described immediately above and in Supplementary Note 3 (step 3). Following this, the fractions were processed into gene expression libraries (according to the Chromium Single-Cell V(D)J Reagent Kits User Guide with 14 cycles of Sample Index PCR) and index sequencing libraries (as described in Supplementary Note 3, steps 4 and 5). For our 5′ sgRNA-CR1^{cs1} experiment, guide molecules were amplified using 0.6 mM oJR163 and oJR166 (5′- CAAGCAGAAGACGGCATACGAGATCATGCCTAGTCTCGTGG GCTCGGAGATGTGTATAAGAGACAGGTACTTGCTAGGACCGGCCTTAAA GC-3′). Because the resulting index library had a contaminating low-molecular weight species (suspected primer dimers) an additional selection for 248–302-bp fragments was performed using a BluePippin (Sage Science) before sequencing.

Hybridization-based target enrichment. To enrich select transcripts from single-cell gene expression libraries for deep sequencing (so-called 'target enrichment'), we developed a hybridization capture protocol. Briefly, using 120-nucleotide biotinylated oligos, which we generated according to specific design criteria outlined in Supplementary Note 5, we performed streptavidin pulldowns of target sequencing amplicons from indexed 10x Genomics gene expression libraries. We tested our enrichment approach in two scenarios: (1) a single library from our dual-guide 3′ direct-capture Perturb-seq experiment to evaluate GIs and (2) all 16 libraries (in two pools of 8) from our multiplexed CRISPRi 3′ direct-capture Perturb-seq experiment. Using the former, we compared deep sequencing of both the unenriched and enriched libraries, and using the latter, we tested the functional use of L1000 transcriptomes. For pooling libraries, we mixed 187.5 ng from each to obtain a total mass of 1,500 ng and dried the library with a SpeedVac. We then followed steps 4 to 7 of the published Twist Biosciences protocol for hybrid capture available at https://www.twistbioscience.com/sites/default/files/resources/2019-01/DOC-001031%20Twist%20Protocol%20Custom%20Panels%20REV%201.0.pdf. This protocol consists of a 16-h probe hybridization at 70 °C, pulldown of hybridized probes using streptavidin beads and five cycles of postcapture PCR before sequencing.

Sequencing. For our UPR direct-capture Perturb-seq experiments, both the gene expression and index sequencing libraries were sequenced using a NovaSeq 6000 S2 Reagent kit (Illumina) and a custom sequencing strategy (26 bp Read 1, 125 bp Read and 8 bp Index Read 1) where the extended Read 2 was used to sequence guide RNA targeting regions in our 5′ guide sequencing libraries. For all other libraries, we sequenced using the standard format for scRNA-seq from 10x Genomics (28 bp Read 1, 98 bp Read 2 and 8 bp Index Read 1) on a NovaSeq 6000 System (Illumina) with NovaSeq 6000 S4 Reagent kits (Illumina).

Data processing, statistics and analysis. We used Cell Ranger 3.0 software (10x Genomics) for alignment of scRNA-seq reads, collapsing reads to UMI counts, cell calling and depth normalization of transcriptome libraries. Index reads were aligned to expected sequences using bowtie for GBC Perturb-seq and bowtie2 for direct-capture Perturb-seq. We observed index alignment rates of 0.82 for GBCs, 0.35 for 3′ sgRNA-CR1^{cs2}, 0.62 for 3′ sgRNA-CR1^{cs1}, 0.71 for 5′ sgRNA-CR1 and 0.62 for 5′ sgRNA-CR1^{cs1} in our UPR direct-capture Perturb-seq experiments. Downstream analyses were performed in Python, using a combination of Numpy, Scipy, Pandas, scikit-learn, pomegranate, polo and seaborn libraries.

Tests for differences in distributions (for example, of capture rates or correlations of guides) were conducted with a two-sided Mann–Whitney *U*-test (scipy.stats mannwhitneyu with use_continuity=True, alternative='two-sided'). Tests for differences in distributions for paired samples (for example, knockdown by single versus multiplexed guides) were carried out with a two-sided Wilcoxon signed-rank test (scipy.stats wilcoxon with zero_method='wilcox', correction=False, alternative='two-sided'). Tests for differential gene expression were performed with a two-sample, two-sided Kolmogorov–Smirnov test and corrected for multiple-hypothesis testing at a false discovery rate of 0.01 using the Benjamini–Yekutieli procedure. As indicated in the text, differentially expressed genes were also identified by random forest classifiers (scikit-learn extremely randomized trees with 1,000 trees in the forest to predict perturbation status). The advantage of this approach is that we assess the similarity of average expression profiles across platforms regardless of the strength of the perturbation because we do not employ a strict cutoff. Correlations reported are Pearson correlation coefficients unless otherwise indicated. Sample sizes used to calculate statistics are provided in the figures and legends. Additional information is available in the Nature Research Life Sciences Reporting Summary linked to this article, and details specific to individual data analyses can be found in Supplementary Note 6.

Perturbation identity mapping. Within our sequencing data, we found evidence of perturbation index reads containing spurious CBC–index pairs. We attribute these to the droplet encapsulation of ambient indexes (GBC transcripts or guides) and PCR chimeras. Therefore, to accurately assign guide identities to cells, true CBC–index pairs had to be determined. For GBC Perturb-seq, we did this using a threshold that separates the bimodal distribution of GBC coverage (reads per UMI) as previously described[4]. However, for direct-capture Perturb-seq, we found that coverage distributions were not bimodal, at least not at the downsampled sequencing depth we used to compare libraries in our UPR experiments (25 million aligned index reads per GBC or guide sequencing library). At this sequencing depth, saturation of the index libraries is 0.75 for GBC, 0.96 for 3′ sgRNA-CR1^{cs2}, 0.71 for 3′ sgRNA-CR1^{cs1}, 0.28 for 5′ sgRNA-CR1 and 0.60 for 5′ sgRNA-CR1^{cs1}. Instead, we found that each guide had a bimodal distribution of the number of UMIs per CBC (capture rates) and that these rates vary across guide RNA targeting regions (perhaps influenced by targeting region-dependent variability in guide stability, Cas9 binding and/or RT efficiency) (Supplementary Fig. 2e,f).

Given targeting region-variable capture rates, to assign guide identities to cells, we fit a two-component mixture model, consisting of a Poisson (lower) and Gaussian (upper) distribution, to the $\log_2$ transformed capture rates (UMIs per CBC) for each guide RNA targeting region, as exemplified in Supplementary Fig. 2b. These mixture models enabled us to separate the upper modes (representing transduced cells) from the lower modes (representing background) and thus assign guides to cells. Each cell with a posterior probability >0.5 of belonging to an upper mode component was assigned a given guide identity. This procedure produced a coherent proportion of cells assigned to each guide identity (Supplementary Fig. 2h) and a coherent multiplet rate across platforms—within 1–1.6-fold of expectations based on library transduction (assuming Poisson infection distribution) and published multiple encapsulation rates (Fig. 1d).

In our UPR experiments, only cells with a single assigned guide were considered for downstream analysis; however, for dual-guide experiments, cells with two assigned guides were used. Across all dual-guide direct-capture Perturb-seq experiments, we observed that >67% of cells contained exactly two sgRNAs. We attribute many of the cells with fewer than two assigned guides to stringent guide assignment cutoffs. For example, given ~90% assignment rate in single-guide experiments (on par with GBC Perturb-seq and CROP-seq), we expect only ~81% of dual-guide cells to be assigned exactly two guides. Yet our mapping strategy is clearly overly conservative as it assumes that guides are independently paired. To increase assignments rates in future applications, our mapping framework could be extended to fit a multivariate mixture model that jointly calls guides by leveraging shared information. Cells with more than two guides, on the other hand, may arise from either multiple infection events or double loading into droplets. Our loading scheme (designed to recover ~15,000 cells per lane) increased these doublets but notably also minimized reagent cost per recovered cell. Last, with direct-capture Perturb-seq, we can identify cells bearing undesired sgRNA pairs (generated from intermolecular lentiviral recombination between programmed pairs[9–12]) and computationally exclude them from downstream analysis. In our data, we observed rates of novel pairs varying from 0.09 to 0.15 across experiments, which is roughly consistent with a previous report[28].

Expression normalization, average expression profiles and target knockdown or activation. We normalized for differences in capture and sequencing coverage across cells by rescaling each cell to have the same total gene expression UMIs (that is, each row of the raw expression matrix is rescaled to have the same sum).

We then *z*-normalized expression of each gene with respect to the mean and standard deviation of that gene in the control cell population. We generated pseudo-bulk RNA-seq phenotypes for individual guides or guide pairs by averaging the normalized expression profiles of well-expressed genes—excluding genes with a mean expression <1 UMI per cell (Figs. 1e and 3e) and <0.5 UMI per cell (Supplementary Fig. 3b) across all cells assigned that guide or guide pair (and excluding multiplets). We computed on-target gene knockdown as the ratio of the mean number of target UMIs in perturbed cells versus the mean number of target UMIs in control cells (bearing nontargeting sgRNAs), and we computed on-target gene activation as the ratio of the mean number of target UMIs in perturbed cells versus the mean number of target UMIs in controls.

Reporting Summary. Further information on research design is available in the Nature Research Reporting Summary linked to this article.

Data availability

Raw and processed sequencing data are available at Gene Expression Omnibus under accession code GSE146194.

Code availability

Cell Ranger 3.0 is available from 10x Genomics (https://support.10xgenomics.com/single-cell-gene-expression/software/downloads/latest). Our previously published analytic framework for Perturb-seq analysis[17] is available at https://github.com/thomasmaxwellnorman/Perturbseq_GI. Python scripts and Jupyter notebooks for direct capture guide identity assignment are available at https://github.com/josephreplogle/guide_calling. Python Jupyter notebooks for the design of hybridization capture probes are available at https://github.com/josephreplogle/target_enrichment.

Acknowledgements

We thank S.E. Vazquez, A. Guna, M. Jost, D. Yang, R. Saunders, X. Qiu, E. Chow, R. Sit and all members of the Weissman and Adamson laboratories and 10x Genomics for helpful discussions. This work was funded by National Institutes of Health grant nos. P50 GM102706, U01 CA168370, R01 DA036858 and RM1HG009490 (all to J.S.W.), the Defense Advanced Research Projects Agency (DARPA) (grant no. HR0011-19-2-0007), the Chan Zuckerberg Initiative and Princeton University. J.S.W. is a Howard Hughes Medical Institute Investigator. J.M.R. is an NIH/NINDS Ruth L. Kirschstein National Research Service Award fellow (no. F31 NS115380). T.M.N. is a fellow of the Damon Runyon Cancer Research Foundation (no. DRG-(2211-15)). J.A.H. is the Rebecca Ridley Kry Fellow of the Damon Runyon Cancer Research Foundation (no. DRG-2262-16). J.C. is funded by the Jane Coffin Childs Memorial Fund for Medical Research and the NIH K99/R00 Pathway to Independence Award (no. GM134154).

Author contributions

J.M.R., T.M.N., J.S.W. and B.A. conceived, designed and interpreted the experiments and wrote the manuscript. J.M.R. and B.A. designed, built and validated modified guide constant regions, expression vectors, dual-guide constructs and libraries. J.M.R. performed Perturb-seq experiments with contributions from B.A., A.X., J.C. and J.Z.C. J.M.R. analyzed Perturb-seq data with support from T.M.N., J.A.H. and B.A. T.M.N. and J.M.R. designed the target enrichment strategy in discussion with I.T.F., J.G.A., L.J.A. and K.A.P. J.M.R. performed the target enrichment experiments and analysis. D.P.R. designed the library of candidate capture sequences. 10x Genomics with E.J.M., J.M.T., D.P.R., N.S. and T.S.M. built the Chromium Single-Cell 3′ Reagent Kits v.3 with Feature Barcoding technology.

Competing interests

10x Genomics was involved in producing this work. I.T.F., J.G.A., L.J.A., K.A.P., E.J.M., J.M.T., D.P.R., N.S. and T.S.M. are employees of 10x Genomics. The Regents of the University of California with T.M.N., J.S.W. and B.A. as inventors have filed patent applications related to CRISPRi/a screening, Perturb-seq and GI mapping. J.S.W. consults for and holds equity in KSQ Therapeutics, Maze Therapeutics and Tenaya Therapeutics; is a venture partner at 5AM Ventures and is a member of the Amgen Scientific Advisory Board. J.M.R. and T.M.N. consult for Maze Therapeutics. B.A. is a member of a ThinkLab Advisory Board for and holds equity in Celsius Therapeutics.

Additional information

Supplementary information is available for this paper at https://doi.org/10.1038/s41587-020-0470-y.

Correspondence and requests for materials should be addressed to J.S.W. or B.A.

Reprints and permissions information is available at www.nature.com/reprints.

nature research

Corresponding author(s): Jonathan S. Weissman, Britt Adamson

Last updated by author(s): Feb 17, 2020

Reporting Summary

Nature Research wishes to improve the reproducibility of the work that we publish. This form provides structure for consistency and transparency in reporting. For further information on Nature Research policies, see Authors & Referees and the Editorial Policy Checklist.

Statistics

For all statistical analyses, confirm that the following items are present in the figure legend, table legend, main text, or Methods section.

n/a	Confirmed
☐	☒ The exact sample size (*n*) for each experimental group/condition, given as a discrete number and unit of measurement
☐	☒ A statement on whether measurements were taken from distinct samples or whether the same sample was measured repeatedly
☐	☒ The statistical test(s) used AND whether they are one- or two-sided *Only common tests should be described solely by name; describe more complex techniques in the Methods section.*
☐	☒ A description of all covariates tested
☐	☒ A description of any assumptions or corrections, such as tests of normality and adjustment for multiple comparisons
☐	☒ A full description of the statistical parameters including central tendency (e.g. means) or other basic estimates (e.g. regression coefficient) AND variation (e.g. standard deviation) or associated estimates of uncertainty (e.g. confidence intervals)
☐	☒ For null hypothesis testing, the test statistic (e.g. *F*, *t*, *r*) with confidence intervals, effect sizes, degrees of freedom and *P* value noted *Give P values as exact values whenever suitable.*
☒	☐ For Bayesian analysis, information on the choice of priors and Markov chain Monte Carlo settings
☒	☐ For hierarchical and complex designs, identification of the appropriate level for tests and full reporting of outcomes
☐	☒ Estimates of effect sizes (e.g. Cohen's *d*, Pearson's *r*), indicating how they were calculated

Our web collection on statistics for biologists contains articles on many of the points above.

Software and code

Policy information about availability of computer code

Data collection	Data was collected using commercially available platforms from 10x Genomics and Illumina. Flow cytometry data was collected using BD FACSDiva software (versions 8.0 and 8.0.1). FACSDiva was also used for cell sorting.
Data analysis	For alignment of scRNA-seq reads, collapsing reads to unique molecular identifier (UMI) counts, cell calling, and depth normalization of mRNA libraries, we used Cell Ranger 3.0 software (10x Genomics, https://support.10xgenomics.com/single-cell-gene-expression/software/downloads/latest). Our previously-published analytic framework for Perturb-seq analysis is available at https://github.com/thomasmaxwellnorman/Perturbseq_GI. Python scripts and Jupyter notebooks for direct capture guide identity assignment are available at https://github.com/josephreplogle/guide_calling. Python Jupyter notebooks for the design of hybridization capture probes are available at https://github.com/josephreplogle/target_enrichment. Downstream analyses were performed in Python, using a combination of Numpy, Pandas, scikit-learn, pomegranate, polo, and seaborn libraries, and are described in the Methods, Supplementary Notes, and/or Figure legends.

For manuscripts utilizing custom algorithms or software that are central to the research but not yet described in published literature, software must be made available to editors/reviewers. We strongly encourage code deposition in a community repository (e.g. GitHub). See the Nature Research guidelines for submitting code & software for further information.

Data

Policy information about availability of data

All manuscripts must include a data availability statement. This statement should provide the following information, where applicable:

- Accession codes, unique identifiers, or web links for publicly available datasets
- A list of figures that have associated raw data
- A description of any restrictions on data availability

Sequencing data generated during this study are available from the authors and will be deposited in a public repository (SRA/GEO).

Field-specific reporting

Please select the one below that is the best fit for your research. If you are not sure, read the appropriate sections before making your selection.

☒ Life sciences ☐ Behavioural & social sciences ☐ Ecological, evolutionary & environmental sciences

For a reference copy of the document with all sections, see nature.com/documents/nr-reporting-summary-flat.pdf

Life sciences study design

All studies must disclose on these points even when the disclosure is negative.

Sample size	For single-cell RNA-sequencing experiments, cells were loaded to recover a median coverage of 200 cells per guide. This coverage was selected based on our previous work, which estimated the number of cells per perturbation required to evaluate gene level and signature level effects on transcription (Dixit et al, 2016), and based on the recommended upper limit of cells per sample lane on the Chromium Controller (https://kb.10xgenomics.com/hc/en-us/articles/360001378811-What-is-the-maximum-number-of-cells-that-can-be-profiled-).
Data exclusions	Subpopulations of cells with low UMI counts or that contained apoptotic cells were removed from select analyses as detailed in the Methods section.
Replication	Replication was performed where indicated. Single-cell RNA sequencing datasets are internally controlled and were not replicated.
Randomization	No randomization was performed. All Perturb-seq experiments were run with the same negative controls.
Blinding	No blinding was performed.

Reporting for specific materials, systems and methods

We require information from authors about some types of materials, experimental systems and methods used in many studies. Here, indicate whether each material, system or method listed is relevant to your study. If you are not sure if a list item applies to your research, read the appropriate section before selecting a response.

Materials & experimental systems

n/a	Involved in the study
☒	☐ Antibodies
☐	☒ Eukaryotic cell lines
☒	☐ Palaeontology
☒	☐ Animals and other organisms
☒	☐ Human research participants
☒	☐ Clinical data

Methods

n/a	Involved in the study
☒	☐ ChIP-seq
☐	☒ Flow cytometry
☒	☐ MRI-based neuroimaging

Eukaryotic cell lines

Policy information about cell lines

Cell line source(s)	GFP+ K562 dCas9-KRAB cells (Adamson et al, 2016), K562 dCas9-KRAB cells (Gilbert et al. 2014), K562 dCas9-SunTag with scFV–VP64 cells (Gilbert et al, 2014), and iPSC Cas9 cells (Mandegar et al., 2016) were constructed as previously described.
Authentication	K562 dCas9-KRAB, GFP+ K562 dCas9-KRAB, and HEK293T cell lines were STR authenticated on 01/25/2019.
Mycoplasma contamination	K562 dCas9-KRAB, GFP+ K562 dCas9-KRAB, K562 dCas9-SunTag with scFV–VP64 cells, and HEK293T cell lines tested negative for mycoplasma on 01/11/2019.
Commonly misidentified lines (See ICLAC register)	None.

Flow Cytometry

Plots

Confirm that:

☒ The axis labels state the marker and fluorochrome used (e.g. CD4-FITC).

☒ The axis scales are clearly visible. Include numbers along axes only for bottom left plot of group (a 'group' is an analysis of identical markers).

☒ All plots are contour plots with outliers or pseudocolor plots.

☐ A numerical value for number of cells or percentage (with statistics) is provided.

Methodology

Sample preparation	K562 cells were analyzed by flow cytometry or purified by fluorescence activated cell sorting after lentiviral transduction and growth in standard culture conditions. BFP expression was used as a marker of successful transduction.
Instrument	Flow cytometry data was collected using one of two LSR II flow cytometers and cell sorting was performed on a FACSAria2 (BD Biosciences).
Software	Flow cytometry data was collected using BD FACSDiva software (versions 8.0 and 8.0.1). FACSDiva was also used for cell sorting.
Cell population abundance	n/a
Gating strategy	SSC/FSC gates were first applied to determine cells. Cells were then gated to separate BFP+ from BFP- cells.

☒ Tick this box to confirm that a figure exemplifying the gating strategy is provided in the Supplementary Information.